coatings

MDPI

Article

Enhancing the Antibacterial Properties of Chitosan Coatings: Ag@Chitosan and Chitosan from Insects

Michela Marsico [1], Rezvan Azari [2], Mariangela Curcio [1], Roberto Teghil [1], Micaela Triunfo [1], Patrizia Falabella [1], Aldo Roberto Boccaccini [2] and Angela De Bonis [1,*]

[1] Department of Science, University of Basilicata, Viale dell'Ateneo Lucano 10, 85100 Potenza, Italy; michela.marsico@unibas.it (M.M.); mariangela.curcio@unibas.it (M.C.); roberto.teghil@unibas.it (R.T.); micaela.triunfo@unibas.it (M.T.); patrizia.falabella@unibas.it (P.F.)

[2] Institute of Biomaterials, Department of Materials Science and Engineering, University of Erlangen-Nuremberg, 91058 Erlangen, Germany; rezvan.azari@fau.de (R.A.); aldo.boccaccini@fau.de (A.R.B.)

* Correspondence: angela.debonis@unibas.it

Abstract: In this study, the electrophoretic deposition (EPD) technique was used to prepare chitosan-based coatings with enhanced antibacterial activity suitable for bone implant applications. We designed, prepared, and compared the physico-chemical and biological properties of coatings obtained with commercial chitosan, chitosan enriched with silver nanoparticles, and chitosan obtained from insects. With the aim to consider the issue of sustainability, silver nanoparticles were directly prepared in the chitosan solution by laser ablation via a liquid technique, avoiding the use of chemicals and limiting the production of wastes. Moreover, a sustainable source of chitosan, such as *Hermetia Illucens* exuviae, was considered. The EPD process was optimized by adjusting parameters like voltage and deposition time to achieve ideal coating thickness and adhesion. The prepared films were characterized by spectroscopic and microscopic techniques such as SEM, XRD, and FTIR. Antimicrobial tests against *E. coli* and *S. aureus* revealed that silver nanoparticles enhanced the antibacterial properties of the polymer, whereas the biological evaluation using the WST8 test on MG63 human osteoblast-like cells showed that all coatings were non-toxic. Finally, chitosan obtained from insect showed comparable properties with respect to the commercial polymer, suggesting it could replace seafood-derived chitosan in biomedical applications, whereas the Ag@chitosan composite demonstrated superior antibacterial activity without compromising its biocompatibility.

Keywords: electrophoretic deposition; chitosan; coating; Ag NPs; antibacterial activity

Citation: Marsico, M.; Azari, R.; Curcio, M.; Teghil, R.; Triunfo, M.; Falabella, P.; Boccaccini, A.R.; De Bonis, A. Enhancing the Antibacterial Properties of Chitosan Coatings: Ag@Chitosan and Chitosan from Insects. *Coatings* **2024**, *14*, 925. https://doi.org/10.3390/coatings14080925

Academic Editor: Simona Liliana Iconaru

Received: 1 July 2024
Revised: 16 July 2024
Accepted: 22 July 2024
Published: 24 July 2024

1. Introduction

In recent years, the development of advanced coatings for bone implants has attracted considerable interest in the field of orthopaedic surgery and biomedical engineering [1]. Bone implant coatings are designed to optimize the process of osseointegration, i.e., forming a stable integration of implants with the surrounding bone tissue. This process involves a series of biological events that allow the implant to merge organically with the surrounding bone, creating a solid and durable connection. Since the interaction at the interface between the bone and implant plays a crucial role in this process, coatings and surface treatments are used to improve cell adhesion and promote osteointegration [2].

Many studies were devoted to proving the capability of advanced materials (such as hydroxyapatite, bioactive glasses, or bioactive polymers) to promote the formation of new bone tissue around implants. Furthermore, by incorporating specific growth factors and biomolecules, it is possible to tune the properties of the coating and enrich its functionalities to stimulate tissue regeneration and to accelerate the healing process [3]. Among deposition techniques, electrophoretic deposition (EPD) has emerged as a promising room-temperature method to achieve precise control over coating properties [4]. EPD offers a versatile approach to accurately deposit uniform and adherent coatings with controlled thickness

and composition. Through EPD, the coating process can be adapted to accommodate various implant geometries and materials, facilitating the customization of implants based on specific patient requirements [5].

EPD also allows to deposit nanocomposite film to obtain coatings that possess the properties of both organic components, such as polymers, and inorganic compounds, such as metals or metal oxides [6]. Polymers derived from nature are commonly used in tissue engineering to create coatings and scaffolds thanks to their compatibility with living tissues and their ability to actively support cell growth and proliferation. Among natural polymer, chitosan (Cs) has favourable characteristics, such as biodegradability, biocompatibility, and low immunogenicity, making it an attractive candidate for biomedical applications [7]. Chitosan is a cationic polysaccharide, a copolymer formed by alternating units of N-acetylglucosamine and D-glucosamine. It is usually obtained via the deacetylation of chitin, the major natural polysaccharide, which is located in the crustaceous and arthropod exoskeleton and in the cell walls of fungi [8]. Beyond its biocompatibility and biodegradability, chitin exhibits good mechanical properties such as high tensile strength and stiffness [9]. However, its applications are limited due to its hydrophobicity and limited solubility. To overcome this drawback, chitin is frequently converted into chitosan, an analogue that is more soluble. Thanks to the possibility to prepare Cs-based materials in different forms, ranging from nanoparticles to thin films to sponges and fibres, this polymer has been proposed for drug delivery, wound healing, and tissue engineering uses [10]. Its antimicrobial and haemostatic activities make it an excellent candidate in dental surgery and conservative dentistry [11]. Moreover, the ability of Cs to promote adhesion, proliferation, and cellular differentiation further increases its suitability for bone tissue engineering [12]. The main source of Cs is waste from the fishing industry, but alternative sources of Cs have recently been considered, of which insects seem to be the most promising [13]. Extracting Cs from insects emerges as a more advantageous process than alternative sources, specifically in terms of the extraction method used, its chemical consumption, production time, and yield [14]. Moreover, it was shown that the integration of Cs and silver nanoparticles (Ag NPs) through electrophoretic deposition has an immense potential to improve the biocompatibility and antimicrobial properties of bone implants [15]. In fact, the presence of Ag NPs enriches the Cs matrix with antimicrobial properties, addressing the widespread problem of implant-related infections, which significantly affect the outcomes of surgical operations in patients [16,17].

Recently, the attention of researchers was focused on the development of green methodologies for the preparation of Ag NPs. Several studies report the use of biological reducing agents such as microorganisms or plant extracts for the production of nanoparticles [18,19]. Laser Ablation in Liquid (LAL) can be considered a sustainable technique and has proven to be a suitable strategy to prepare the NPs of metals, oxides, and alloys with a composition and morphology depending on the physico-chemical properties of the target and the liquid, as well as on the parameters of the laser source [20].

LAL is based on the ablation of a solid target in a liquid environment. When an intense laser pulse hits a solid surface, the local evaporation of the target takes place with the formation of laser-induced hot plasma that is confined in the liquid environment. The evaporation of the surrounding liquid leads to the formation of a Cavitation Bubble (CB), characterized by oscillating dynamics. The NPs nucleate and grow in the CB and are released into the liquid when the bubble collapses [21].

This study reports on the production and characterisation of coatings for metallic bone implants using EPD. The physico-chemical and functional properties of films obtained by depositing Ag@Cs and Cs from insects were compared with those of films obtained by depositing commercial Cs under the same experimental conditions.

2. Materials and Methods

2.1. Materials and Processing

Cs solutions (1g/L) were prepared by dissolving low-MW Cs (100–300 kDa, 70% deacetylation degree, purchased from Acros, Thermal Fisher Scientific, Waltham, MA, USA) in 0.1% acetic acid (pH = 4.2). The solutions were kept under agitation at a temperature of 35 °C for 4 h until a complete Cs dissolution. The same procedure was followed to prepare the 1g/L solution by using Cs obtained from *Hermetia illucens* exuviae (35–40 kDa, 90% deacetylation degree) (CsE) [22].

Ag NPs were prepared by LAL technique. A nanosecond Nd:YAG laser source, (wavelength of 532 nm, pulse duration of 7 nm, repetition frequency of 10 Hz and power of 150 mW) was focused vertically on the Ag target (Goodfellow) using a 5 mm lens. The column of liquid above the target surface was fixed at 2 cm. Colloidal solutions (Ag NPs@Cs) with a concentration of Ag NPs of 8 µg/mL were obtained for ablation time of 45 min.

316L stainless steel foils of 0.2 mm thickness were used as electrodes for the EPD process. The electrodes (3 × 1.5 cm) were cleaned with acetone and isopropanol mixture before the deposition. Moreover, 1g/L Cs, 1g/E-Cs, and Ag NPs@Cs solutions were kept in agitation for about one hour before deposition. Direct current EPD was used for voltage ranging from 30 V to 10 V using a TTi power supply (EX752M Multi-mode PSU, Aim and Thurlby Thandar Instruments, Cambridgeshire, UK) for different deposition times. The experimental conditions used for the depositions are reported in Table 1.

Table 1. EPD parameters for the coating deposition experiments.

Coating	Solutions	ddp	Electrode Distance	Dep. Time
Cs-30V	Cs	30 V	1 cm	1 min
Cs-20V	Cs	20 V	1 cm	1 min
Cs	Cs	10 V	1 cm	1 min
Ag-Cs30	Ag NPs@Cs	10 V	1 cm	30 s
Ag-Cs45	Ag NPs@Cs	10 V	1 cm	45 s
Ag-Cs1	Ag NPs@Cs	10 V	1 cm	1 min
Ag-Cs2	Ag NPs@Cs	10 V	1 cm	2 min
CsE	CsE	10 V	1 cm	1 min

2.2. Physico-Chemical Characterization

The morphology and size distribution of Ag NPs were determined using transmission electron microscopy (TEM) via a G2 20 FEI Tecnai instrument (FEI company, Hillsboro, OR, USA). For this, some drops of the Ag NPs@Cs solution were dropped on a Holey carbon-coated copper grid (Agar Scientific Ltd., Essex, UK). Uv-vis absorption spectra were obtained by a Specord 50/PLUS Analytic Jena spectrophotometer (Analytik Jena, Jena, Germany). All spectra were acquired in the 200 to 800 nm range. IR characterization of the coatings was carried out by a Nicolet 6700 spectrometer (Thermal Fisher Scientific, Waltham, MA, USA) operating in ATR mode, in the 4000 to 400 cm^{-1} range. The XRD diffractograms were obtained using the Rigaku (MiniFlex 600, Rigaku Corporation, Tokyo, Japan) diffractometer, using Cu-Kα radiation at 40 kV and 32 mA. Diffraction patterns were acquired in the 2θ range of 5°–60°, with a step size of 0.040° and a time per step of 4 s. The wetting properties were evaluated by contact angle measurement for each coating using the KRÜSS DSA30 (KRÜSS Scientific, Hamburg, Germany) drop shape analyser. Five drops of distilled water with a volume of 3 µL were dropped on the centre of each sample to avoid any effects from the edges. Then, the mean value and the standard deviation of the contact angle were calculated. A scanning electron microscope (SEM) equipped with an energy dispersive X-ray (EDX) analyser (SEM Carl Zeiss Auriga (Carl Zeiss, Jena, Germany) with EDS, X-MaxN Oxford Instruments (Oxford Instruments, Abingdon, UK)) was used to study the surface morphology, elemental composition, and thickness of coatings. The

thickness of each deposit was evaluated at 3 points along the cross-section of coatings, and the Ag percentage was measured at 8 points on the coatings' surfaces. The mechanical properties of the coatings were evaluated qualitatively through cyclic bending test. During this test, the coated substrate was bent around an axis of 180° until the coated surface became parallel to the other half of the substrate. Subsequently, the substrate was folded back to its original position before starting the next bending cycle. Over the entire process, the distance between the two halves of the folded substrate was maintained constantly less than 2 mm [23].

2.3. Antibacterial Activity

The antibacterial activity of coatings against the Gram-positive bacteria *Staphylococcus aureus* (*S. aureus*) and Gram-negative *Escherichia coli* (*E. coli*) was evaluated. A suspension of *S. aureus* and *E. coli* bacteria was inoculated into a sterile Lysogeny broth (LB) medium overnight. The optical density was then adjusted to 0.015. Aliquots of the bacterial suspensions were added to the samples, previously disinfected by UV, and immersed in sterile LB; uncoated stainless steel was used as the control. After a 24 h incubation period at 37 °C, these extracts were completely homogenised. Then, 100 µL was collected from each extract and placed in a 96-well plate for the analysis. A second test was performed by incubating the coating for 24 h at 37 °C in sterile culture medium before the inoculation of bacterial strains. A microplate reader (PHOmo, anthos Mikrosysteme GmbH, Schwerin, Germany) was used for optical density measurements at 600 nm.

2.4. Cell Viability Test

For the viability test, MG63 cells (human osteosarcoma cell line) were use as model cells. This cell line is commonly used to characterize biomaterials intended to be in contact with bone, as MG-63 cells express many characteristics of normal osteoblasts [24]. Cells were cultured in cell culture polystyrene flasks using Dulbecco's modified Eagle's medium (DMEM, Gibco, Schwerte, Germany), supplemented with 10 vol. % fetal bovine serum (FBS, Sigma-Aldrich, Burlington, MA, USA) and 1 vol.% penicillin/streptomycin (Pen-Strep; Sigma-Aldrich, Burlington, MA, USA). After UV treatment, the coatings were placed in a 24-well plate, and 1×10^4 cells were seeded in each well on the sample surface and incubated at 37.5% CO_2 for 24 h, 48 h, and 72 h. Each coating was tested in triplicate. At the end of the incubation time, the culture medium was removed and washed with phosphate-buffered solution (PBS); then, 300 µL of WST-8 reagent (1% reagent solution WST-8 (Sigma-Aldrich, Burlington, MA, USA) and 99% complete fresh medium) was added to each well, and the cells were incubated for ~2 h at 37 °C and 5% CO_2. After incubation, 100 µL of the solution was transferred from each well to a 96-well plate. The absorbance was measured at 450 nm using an Omega FLUO star microplate reader (BMG Labtech, Ortenberg, Germany) UV–Vis spectrometer.

2.5. Statistical Analysis

The experimental results are represented as the mean value ± standard deviation (SD) for each group of samples. The statistical significance between control and samples was analysed using OriginLab 2018 SR1 software (OriginLab Corporation, Northampton, MA, USA). Statistical analysis was performed using one-way ANOVA test with Tukey's post hoc tests, with a probability of $p < 0.05$ considered as being statistically significant.

3. Results

3.1. Ag NPs@Cs Composite

The nanosecond LAL technique was used to directly generate Ag NPs in the polymer solution. The presence of Ag NPs in the Cs solution was confirmed by surface plasmon resonance (SPR), where the band of silver was centred at 403 nm, as reported in Figure 1a.

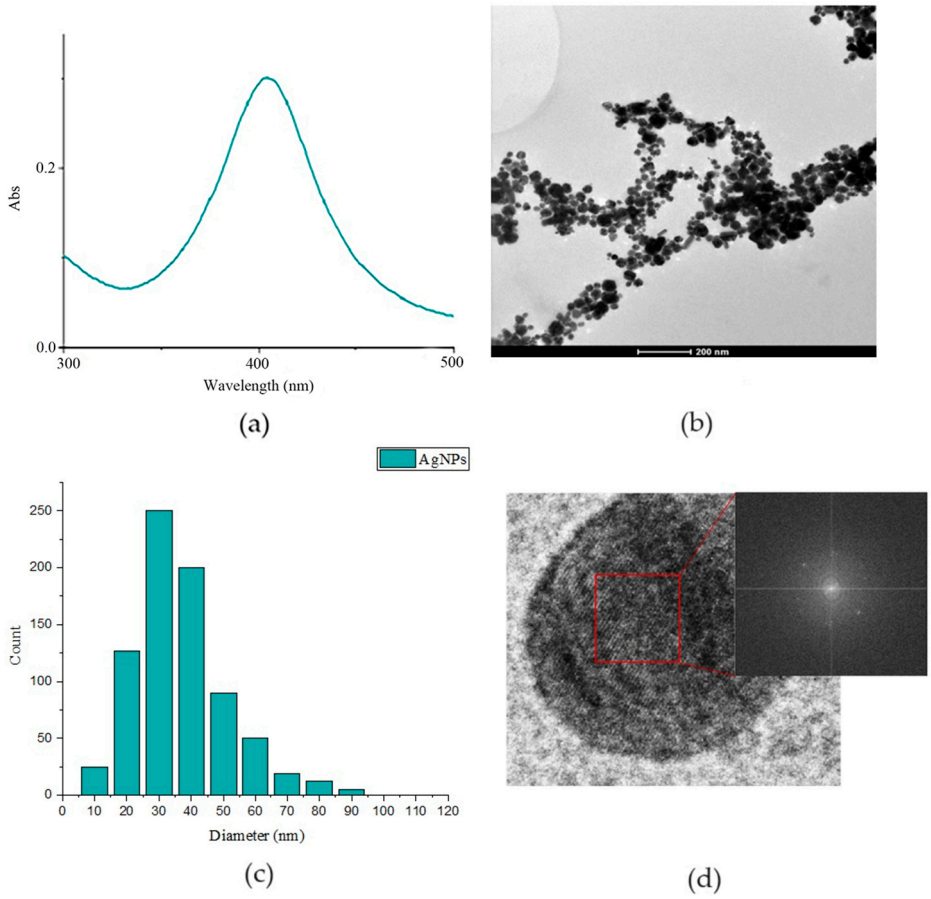

Figure 1. Ag NPs@Cs. (**a**) UV-Vis spectrum; (**b**) TEM image; (**c**) size distribution of silver nanoparticles; (**d**) HR-TEM and FFT of a single Ag particle.

TEM analysis allows to observe spherical NPs with a mean diameter of 30 ± 13 nm, as shown in Figure 1b,c. The presence of a few larger particles (with a diameter of several tens of nanometres) can be related to secondary melting effects due to the re-irradiation of the colloidal solution [25]. Crystalline domains are clearly visible in larger, edge-shaped particles. A lattice distance of 0.24 nm, evaluated by fast Fourier transformation (FFT), matches the (111) lattice distance of the FCC crystal structure of silver (Figure 1d).

3.2. Coatings

Physico-Chemical Characterizations

All coatings were prepared via EPD, as described in Table 1, and were characterized by FTIR, XRD, and SEM techniques.

First of all, we studied the effect of the applied voltage on the chitosan coatings' morphology (Figure 2).

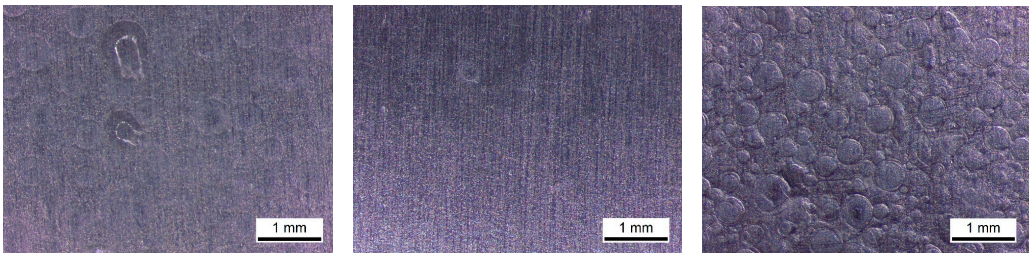

(**a**) (**b**) (**c**)

Figure 2. SEM images of (**a**) Cs-30V, (**b**) Cs-20V, and (**c**) Cs coatings obtained via EPD.

The presence of ripples is clearly visible on the surface of coatings deposited at 30V and 20V. On the other hand, films deposited at 10V are compact and uniform, with this voltage value being used to prepare all the other samples.

The FTIR spectra of Cs, CsE, Ag-Cs1, and Ag-Cs2 are reported in Figure 3a. All coatings present all the signals characteristic of Cs functional groups. In particular, the broad band at 3400 cm^{-1} is associated with the stretching vibrations of O-H and N-H groups. The peaks at 2870 cm^{-1} and 1374 cm^{-1} correspond to the asymmetric stretching vibrations of the aliphatic CH groups and the symmetric deformation vibrations of the CH_3 groups, respectively. Other distinctive peaks are the OH bending vibration at 1430 cm^{-1} and the C=O stretching peaks of amides I and II at 1673 cm^{-1} and 1590 cm^{-1}, respectively [26].

The X-ray diffraction patterns of Cs, CsE, Ag-Cs1, and Ag-Cs2 are reported in Figure 3b. All coatings present a broad band cantered at 20° that can be related to Cs [27]. Moreover, in the XRD spectra of Ag-Cs1 and Ag-Cs2, a weak signal at 2θ 37.8° can be observed, which can be associated with FCC Ag (JPD 01-089-3722). The intensity of this peak increases with the increase in the deposition time.

The wetting and hydrophobicity properties of coatings were evaluated through a water contact angle measurement. Usually, lower contact angles indicate lower hydrophobicity or better wettability. The stainless steel used as a substrate has a contact angle ranging from 90° to 100°. Moreover, the presence of coatings improves wettability by lowering the contact angle. More specifically, Cs and CsE have a contact angle between 60° and 70°. As shown in Figure 3c, the deposits obtained from the Ag NPs@Cs solution show a trend that is in agreement with the deposition time: as time increases, there is a decrease in the contact angle values, ranging from 80° ± 5° to 70° ± 7° to 65° ± 5° for depositions of 30 s, 45 s and 1 min, and 2 min, respectively. Several studies indicate that to achieve the best cellular adhesion, the contact angle of the coatings should be within the range of 40° to 70° [28]. However, it is important to note that this range may vary depending on the type of cell considered [29]. In the context of bone cells, specifically, it has been suggested that the ideal range is between 35° and 85°, with an optimal value of 55° [30]. As a result, while the contact angle of all coatings is within the suitable range, we found that Ag-Cs coatings tend to approach the upper limit of this value.

All coatings present a similar compact and homogeneous surface morphology, as can be observed in the SEM images reported in Figure 4a–f. Some shallow cracks were present in all deposits, and these cracks became sharper and deeper for CsE and Ag-Cs2. Via SEM cross-section analysis, it was possible to evaluate the thicknesses of the various coatings studied (Table 2). A direct correlation between deposition time and thickness could be argued. EDX analysis confirmed that Ag NPs were successfully transferred during the EPD process with an Ag w/w% ranging from 0.8 to 1.2, as reported in Table 2.

Table 2. Thickness and Ag percentage for all coatings.

Sample	Thickness	Ag%
Cs	4.1 ± 0.2 µm	-
Ag-Cs30	2.9 ± 0.7 µm	0.8 ± 0.5
Ag-Cs45	5.1 ± 0.8 µm	1.2 ± 0.5
Ag-Cs1	7.1 ± 0.1 µm	1.0 ± 0.4
Ag-Cs2	14.4 ± 0.7 µm	0.8 ± 0.3
CsE	4.1 ± 0.3 µm	

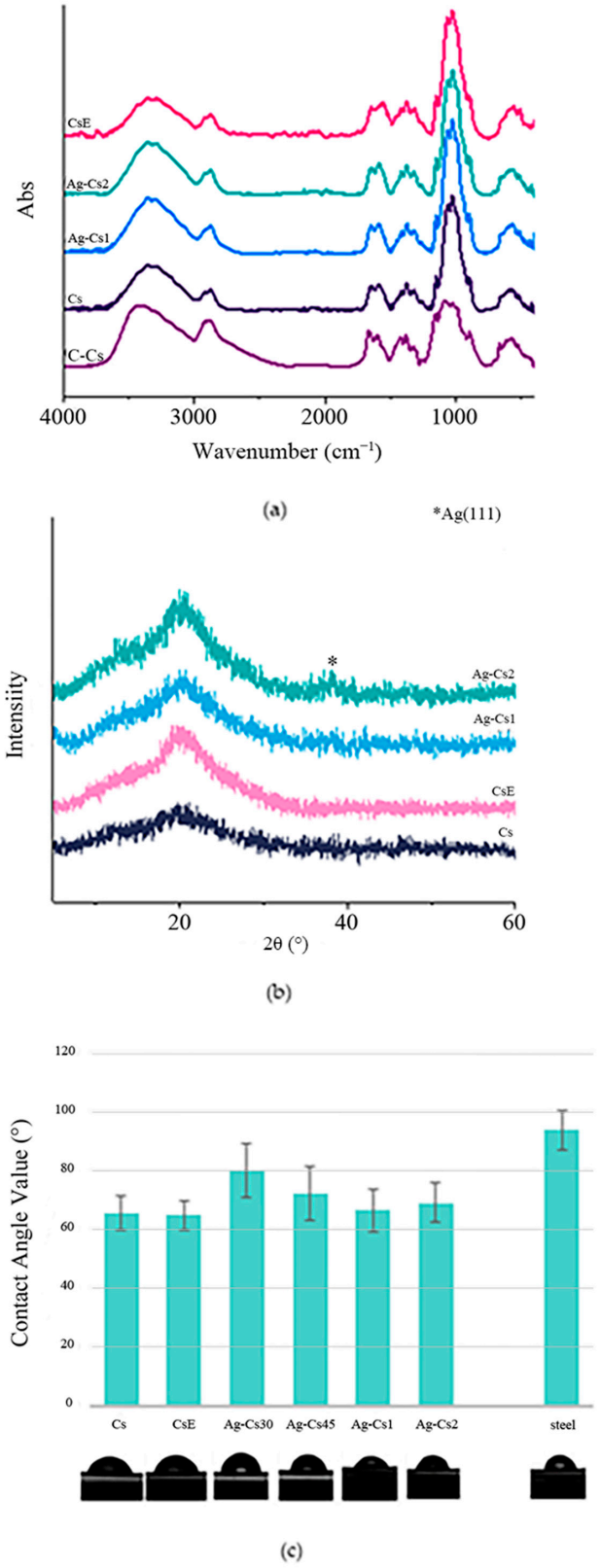

Figure 3. (**a**) FTIR spectra and (**b**) XRD patterns of Cs, CsE, Ag-Cs1, and Ag-Cs2 coatings, respectively, in blue, pink, light blue, and green. (**c**) Average contact angle and profiles (at the bottom of the figure) of the water droplets on Cs, CsE, Ag-Cs30, Ag-Cs45, Ag-Cs1, Ag-Cs2, and uncoated steel immediately after deposition.

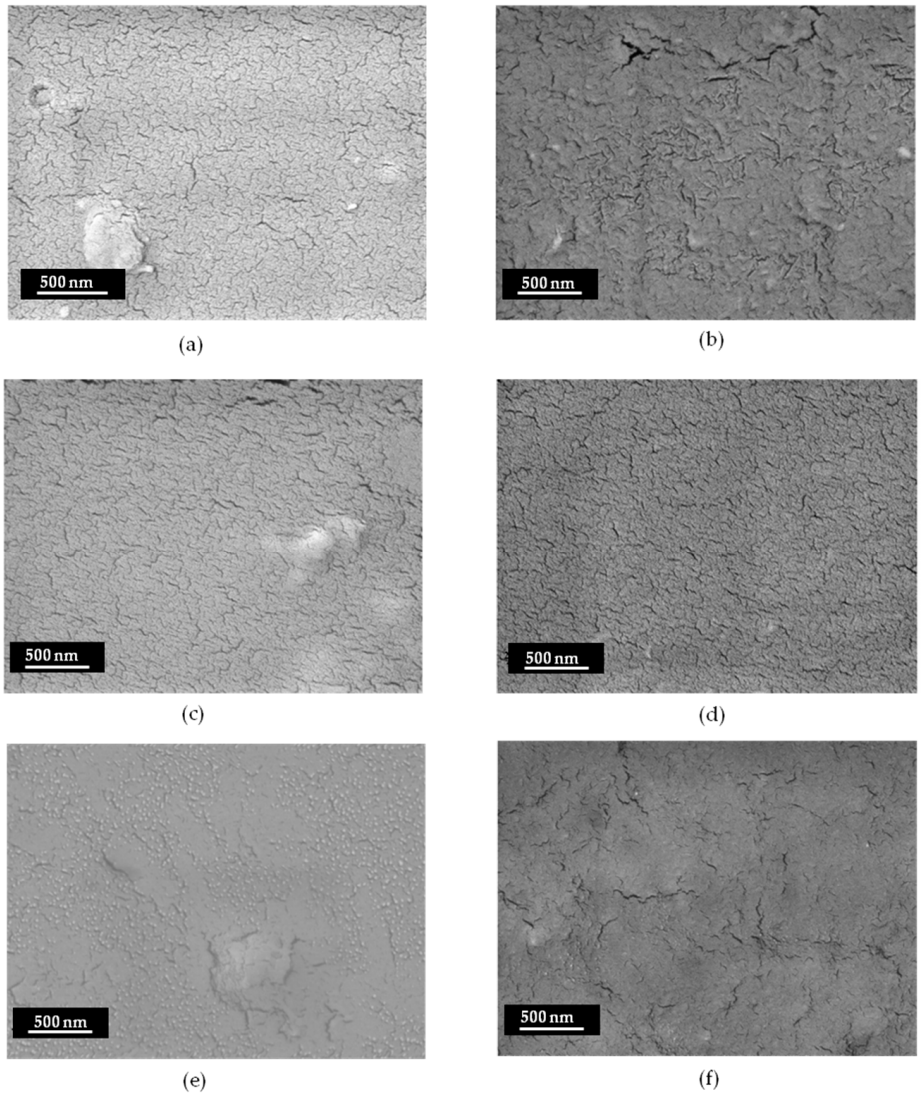

Figure 4. SEM images of (**a**) Cs, (**b**) CsE, (**c**) Ag-Cs30, (**d**) Ag-Cs45, (**e**) Ag-Cs1, and (**f**) Ag-Cs2 coatings obtained via EPD.

To assesses the adhesion of the coatings, the cyclic bending test was used [23]. Figure 5a–f displays the cyclically bent coatings in the region where tensile strength is at the maximum. After 10 bending cycles, Cs and CsE samples showed a relatively compact surface with few micro-cracks and loose areas on the edges of the coating. No visible cracks or detachments were observed after 10 bending cycles for the Ag-Cs45 coating, and only a few cracks and some slight lifting were present for the Ag-Cs30 and Ag-Cs1 coatings. On the other hand, the Ag-Cs2 coating clearly showed many cracks and lifting after 10 bending cycles.

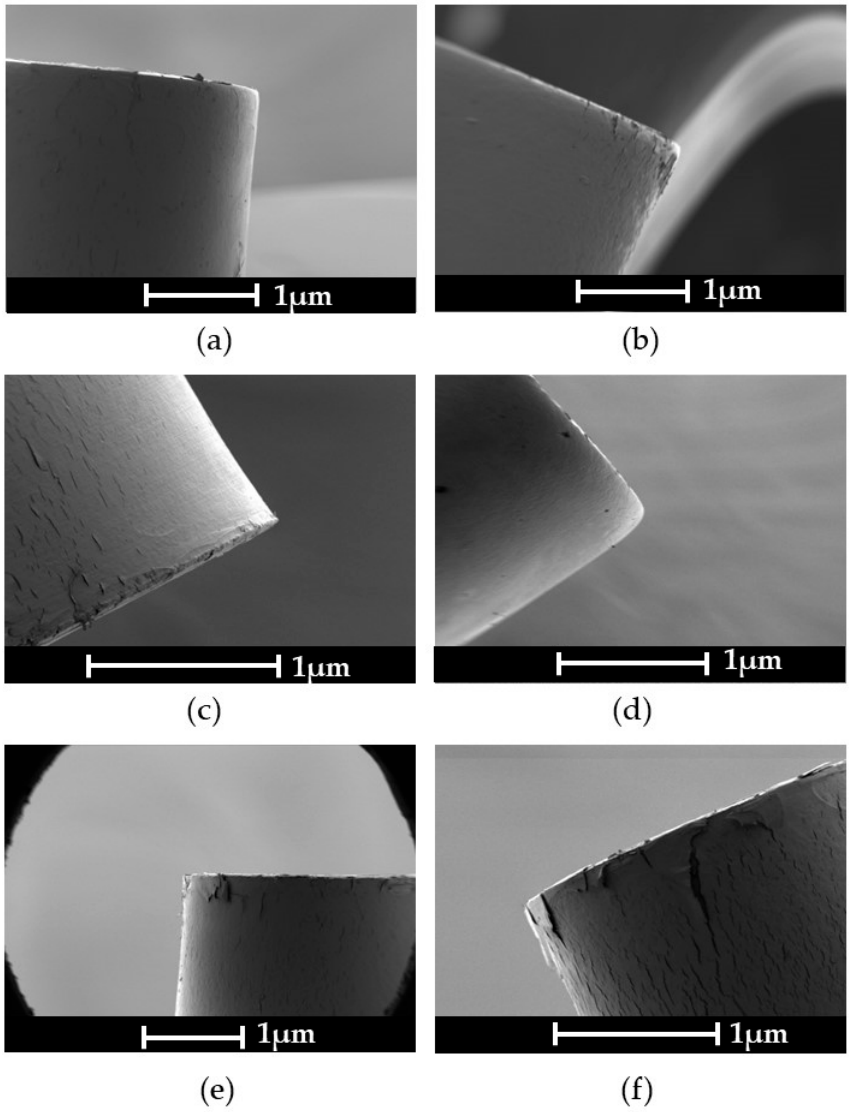

Figure 5. SEM images of stainless steel coated with (**a**) Cs, (**b**) CsE, (**c**) Ag-Cs30, (**d**) Ag-Cs45, (**e**) Ag-Cs1, and (**f**) Ag-Cs2 after 10 bending cycles.

3.3. Antibacterial Activity

The results of the antimicrobial test showed that all coatings tested exhibited an inhibitory effect on bacterial proliferation, both on *S. Aureus* Gram-positive and on *E. Coli* Gram-negative bacteria, as reported in Figure 6a, with a decrease in growth of 15% for all coatings except for the Ag-Cs1 coating, which showed 25% inhibitory activity. The results are in accordance with those reported in similar works [15,31]. After 24 h of incubation in the culture medium, an increase in the limitation of proliferation that exceeded 20% for all coatings was evident, except for the Ag-Cs1 coating, which showed the best result by exhibiting 35% inhibitory activity (Figure 6b). The Ag-Cs1 sample proved to have the best bactericidal performance in both tests. CsE and Cs samples showed comparable antimicrobial activity in both tests, confirming that the antibacterial activity of commercial chitosan and chitosan obtained from the *Hermetia Illucens* exuviae is comparable [32].

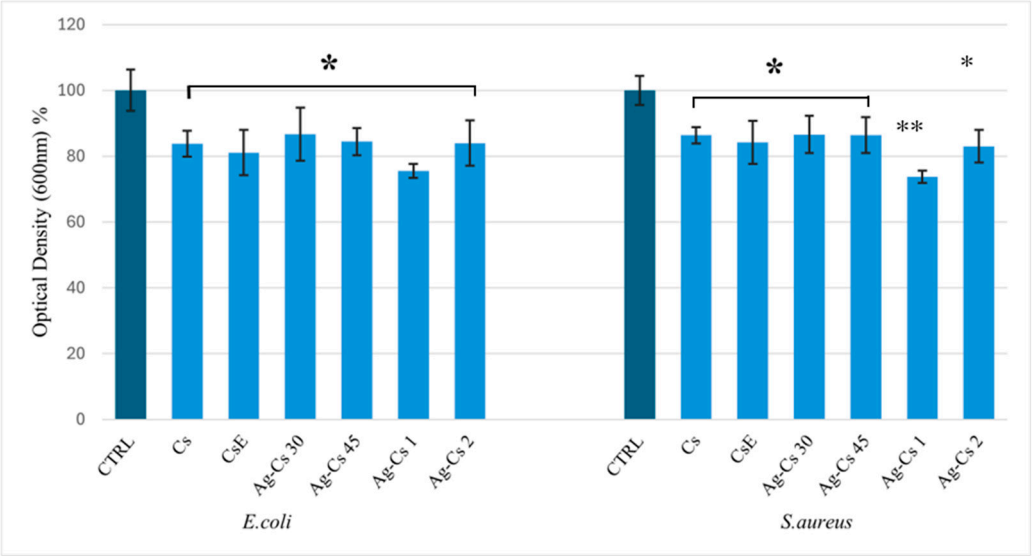

(a)

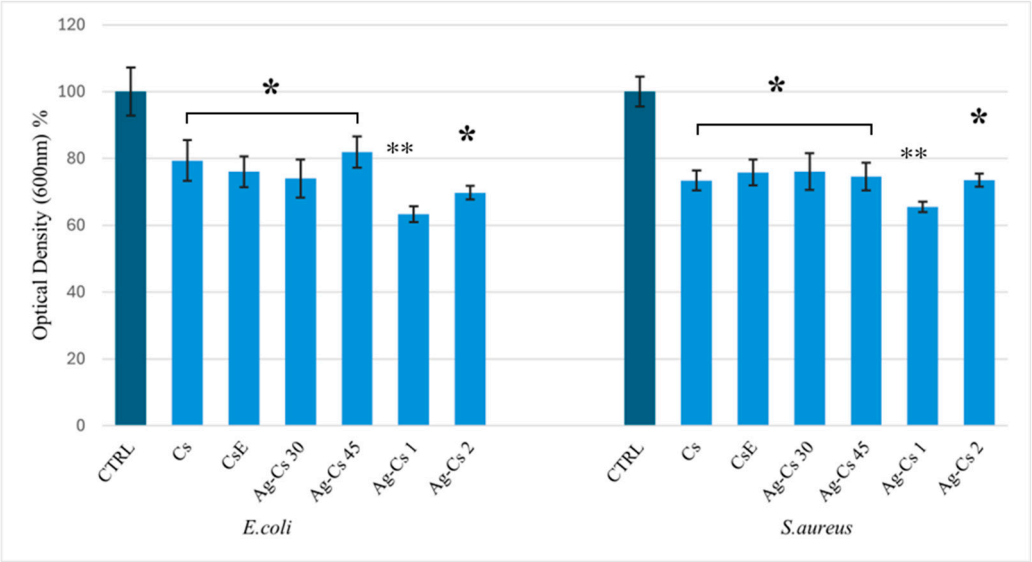

(b)

Figure 6. (**a**) Antibacterial activity of coatings relative to stainless steel against *E. coli* and *S. aureus* after 24 h of incubation. (**b**) Antibacterial activity of coatings relative to stainless steel, preincubated for 24 h, against *E. coli* and *S. aureus* after 24 h of incubation. Asterisks (*) denote significant differences ($p < 0.05$); (**) denote significant differences ($p < 0.01$).

3.4. Viability Test

The cell viability test was performed on human osteoblast-like cells (MG-63) at three different times (24 h, 48 h, and 72 h) and by using uncoated stainless steel as a control (Figure 7). In the 24 h test, the data show reductions of 10–15% in mitochondrial cell activity in the Cs and CsE samples compared to the control. The Ag-Cs30, Ag-Cs45, and Ag-Cs1 coatings showed viability values ranging from 80% to 75%; these deposits prove not to be toxic to the MG-63 cell line. Ag-Cs2's cellular viability was below 60%. This was probably due to an excess release of silver ions in the culture medium, which possibly slowed down cell proliferation by interacting with cellular metabolism [33].

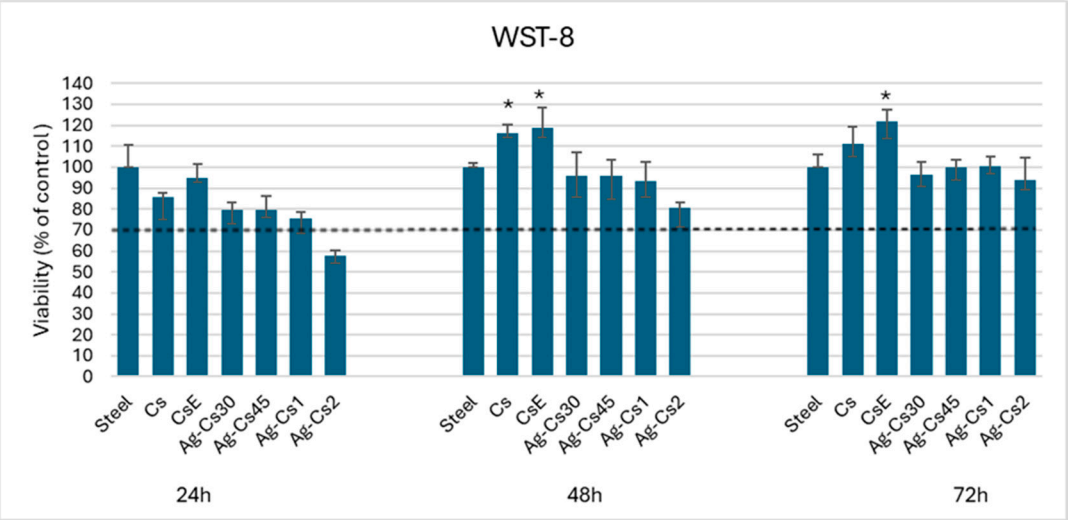

Figure 7. Cell viability of osteoblast-like cells (MG-63) cultured on coatings after 24 h, 48 h, and 72 h of incubation. Stainless steel was used as a control. Asterisks (*) denote significant differences ($p < 0.05$).

In the 48h test, the Cs and CsE coatings provided a substrate with adhesion and proliferation that were slightly better than the control, with a cell viability value of about 117% and 119%, respectively. On the other hand, the Ag-Cs30, Ag-Cs45, and Ag-Cs1 deposits showed values comparable to the control, and the Ag-Cs2 coating showed a cell viability value of around 80%. Finally, in the 72h test, the Cs and CsE samples showed cell proliferation with viability values of 110% and 120%, respectively. At the same time, the deposits of Ag-Cs30, Ag-Cs45, Ag-Cs1, and Ag-Cs2 showed values comparable to the control.

4. Discussion

The LAL technique has been widely used as a sustainable synthetic strategy to produce nanoparticles with a controllable composition, crystallinity, and size distribution [34]. The possibility to enrich the properties of polymers with metallic nanoparticles generated directly in the polymeric solution using LAL has been recently proposed [35]. During the ablation of the Ag target, the nucleation and growth of metallic NPs takes place. However, since laser-induced plasma is strongly spatially and temporally confined [36], the ablation process does not modify the structure of the polymer, enabling it to retain its functional groups and crystallinity—as confirmed via FTIR and XRD analyses (Figure 3a,b). The obtained Ag@Cs colloidal solution was used to coat 316 L stainless steel using the EPD technique. The applied voltage and the deposition times were modified in order to obtain films that were compact and that adhered well to the substrate. Films deposited at higher voltages presented circular ripples (Figure 2a,b). In fact, during electrophoretic deposition, the hydrolysis of water led to the formation of gaseous hydrogen, which can be entrapped in the solution and negatively affect the growth of the deposits [37]. This effect was minimized by operating at a lower voltage. The deposition time was varied in order to vary the thicknesses of the coatings. However, a detachment of the coatings during the cyclic bending test was for the thicker film (Ag-Cs2), probably due to the lower flexibility of the coating. Therefore, the Ag-Cs1 coating seems to be an ideal compromise to achieve compact and homogeneous films that are highly adhesive to substrates. According to the literature, chitosan coatings with thicknesses ranging from 0.2 to 100 μm are suitable for orthopaedic applications. In particular, coatings thinner than 30 μm are appropriate to provide a biocompatible surface that supports cell adhesion and proliferation without significantly altering the implant's mechanical properties [38].

In order to study the antibacterial activity of the prepared coatings, all samples were previously irradiated with UV light. This disinfection technique has a distinct sporicidal and virucidal effect [39] and is preferable with respect to other high-temperature techniques due to the thermal properties of polymers [40]. Ag-Cs films present higher antibacterial activities with respect to undoped coatings, due to the well-known properties of silver [18]. Moreover, we observed that the prolonged contact between the coatings and the medium enabled a stronger inhibitory action to be elicited against the tested bacterial strains, with this effect being greater for Ag-Cs1.

Chitin and chitosan from insects represent a sustainable alternative to overcoming seasonal and regional variations in the availability of crustacean chitosan. For example, chitin and chitosan from *H. Illucens* pupal exuviae are by-products of industrial-scale breeding for the production of new proteins for animal feed [8]. The physico-chemical and functional properties of these biopolymers from H.I exvuviae were investigated and compared to commercial ones [8,22]. CsE and Cs films, deposited in the same experimental conditions, have the same thickness, morphology, substrate adhesion, and antibacterial activity.

The suitability of the deposited films for bone tissue engineering was investigated with a cell viability test performed on human osteoblast-like cells (MG-63). In the 24 h test, a reduction in mitochondrial cell activity for all samples was observed. However, chitosan has been shown to not be toxic to MG-63 cells [41], so it is assumed that the reason for this decrease in viability may be related to the relatively low number of cells attached. It is known that cellular adhesion first involves non-specific forces, such as electrostatic or van der Waals forces, followed by specific interactions with the substrate, which are mediated by cell receptors [42]. However, chitosan lacks specific domains to integrate with receptors or cell recognition sequences (such as RGD) that promote cellular adhesion [43]. As a result, fewer cells are likely to attach to the coating surfaces only through non-specific electrostatic interactions between the protonated amine groups of the glucosamine unit in chitosan and the negatively charged groups of the carboxylate and sulphate in proteoglycans on the cell surface [44]. With increasing the test time (at 48 h and 72 h), Cs and CsE coatings can be identified to be suitable substrates for cell growth, compared to the control. This is partly due to the fact that their contact angles are within the optimal range for cellular adhesion, i.e., from 40° to 70° [28], as well as due the ability of chitosan to stimulate cell growth [45]. The comparison also shows how the CsE coating stimulates proliferation more strongly than Cs at all time points. This is probably linked to the degree of acetylation. In a previous study, it has been shown that the degree of acetylation affects cell adhesion and proliferation; low degrees of acetylation are the best substrates for the proliferation of the MG-63 cell line [46]. In the 72 h test, all the Ag-Cs films presented a cell viability value comparable to a stainless steel substrate.

The enrichment of chitosan with Ag NPs improves the antibacterial properties of the polymer; however, the burst release of ions at the time of first contact with the biological medium can occur at the point when reduced cell activity is observed for all Ag-Cs coatings in the 24 h test [47]. This effect is mitigated at longer durations, with the Ag-Cs films displaying the same behaviour as the control at extended periods as well. The results of this study point to LAL being an eco-sustainable strategy to enrich chitosan with Ag NPs. The deposited films have enhanced antibacterial activity, making them more effective compared to undoped chitosan. Moreover, we have demonstrated that chitosan obtained from the pupal exuviae of *H. Illucens* can be considered as a valuable substitute for commercial chitosan in the EPD coating of stainless steel substrates. However, further data are needed to confirm the suitability of the proposed coatings for bone implant treatment.

5. Conclusions

Commercial chitosan (from maritime origin), chitosan from an alternative source (*Hermetia illucens* exuviae), and chitosan enriched with silver NPs obtained using laser synthesis in a polymeric solution (Ag NPs@Cs) were chosen to be used as samples for coating 316 L stainless steel substrates with the EPD method. The optimization of de-

position parameters allowed for the deposition of adherent and uniform coatings with controlled thicknesses. All the coatings showed antibacterial properties that effectively limited bacterial growth on both Gram-positive and Gram-negative strains, with the Ag-Cs1 coating showing the highest antibacterial activity. All coatings led to there being an effective interaction with osteoblast-like cells, which are non-cytotoxic. Furthermore, Cs and CsE revealed not only that they lack toxicity but also that they lack the ability to promote cell proliferation compared to stainless steel. Moreover, the CsE sample showed a better cellular compatibility profile at all incubation times compared to commercial Cs. Considering the above information, this study paves the way for the use of alternative sources, such as chitosan and chitosan enriched with silver nanoparticles, as antibacterial coatings for biomedical implants.

Author Contributions: Conceptualization, M.M., M.C., A.D.B. and A.R.B.; methodology, M.M., M.C. and R.A.; validation, A.D.B., M.T. and P.F.; investigation, M.M.; resources, M.T., P.F. and A.D.B.; data curation, M.M., M.C. and A.D.B.; writing—original draft preparation, M.M., M.C. and A.D.B.; writing—review and editing, R.A. and A.R.B.; supervision, A.R.B., R.T. and A.D.B.; project administration, A.D.B. and A.R.B.; funding acquisition, A.D.B. All authors have read and agreed to the published version of the manuscript.

Funding: Rezvan Azari would like to thank the German Academic Exchange Service (DAAD) for granting her a scholarship to pursue her doctoral studies.

Institutional Review Board Statement: Not applicable.

Informed Consent Statement: Not applicable.

Data Availability Statement: Data are contained within this article.

Conflicts of Interest: The authors declare no conflicts of interest.

References

1. Zhang, B.G.X.; Myers, D.E.; Wallace, G.G.; Brandt, M.; Choong, P.F.M. Bioactive coatings for orthopaedic implants-recent trends in development of implant coatings. *Int. J. Mol. Sci.* **2014**, *15*, 11878–11921. [CrossRef] [PubMed]
2. Bohara, S.; Suthakorn, J. Surface coating of orthopedic implant to enhance the osseointegration and reduction of bacterial colonization: A review. *Biomater. Res.* **2022**, *26*, 1–17.
3. Joshi, M.U.; Kulkarni, S.P.; Choppadandi, M.; Keerthana, M.; Kapusetti, G. Current state of art smart coatings for orthopedic implants: A comprehensive review. *Smart Mater. Med.* **2023**, *4*, 661–679. [CrossRef]
4. Long, S.; Zhu, J.; Jing, Y.; He, S.; Cheng, L.; Shi, Z. A Comprehensive Review of Surface Modification Techniques for Enhancing the Biocompatibility of 3D-Printed Titanium Implants. *Coatings* **2023**, *13*, 1917. [CrossRef]
5. Boccaccini, A.R.; Keim, S.; Ma, R.; Li, Y.; Zhitomirsky, I. Electrophoretic deposition of biomaterials. *J. R. Soc. Interface* **2010**, *7* (Suppl. S5), S581–S613. [CrossRef] [PubMed]
6. Zhitomirsky, I. Electrophoretic deposition of organic-inorganic nanocomposites. *J. Mater. Sci.* **2006**, *41*, 8186–8195. [CrossRef]
7. Jiménez-Gómez, C.P.; Cecilia, J.A. Chitosan: A Natural Biopolymer with a Wide and Varied Range of Applications. *Molecules* **2020**, *25*, 3981. [CrossRef]
8. Triunfo, M.; Guarnieri AIanniciello, D.; Coltelli, M.B.; Salvia, R.; Scieuzo, C.; De Bonis, A.; Falabella, P. A comprehensive characterization of Hermetia illucens derived chitosan produced through homogeneous deacetylation. *Int. J. Biol. Macromol.* **2024**, *271*, 132669. [CrossRef]
9. Yosri, N.; Khalifa, S.A.M.; Attia, N.F.; Du, M.; Yin, L.; Abolibda, T.Z.; Zhai, K.; Guo, Z.; El-Seedi, H.R. Sustainability in the green engineering of nanocomposites based on marine-derived polysaccharides and collagens: A review. *Int. J. Biol. Macromol.* **2024**, *274*, 33249. [CrossRef]
10. Iqbal, Y.; Ahmed, I.; Irfan, M.F.; Shahid Chatha, S.A.; Zubair, M.; Ullah, A. Recent advances in chitosan-based materials; The synthesis, modifications and biomedical applications. *Carbohydr. Polym.* **2023**, *321*, 121318. [CrossRef]
11. Paradowska-Stolarz, A.; Mikulewicz, M.; Laskowska, J.; Karolewicz, B.; Owczarek, A. The Importance of Chitosan Coatings in Dentistry. *Mar. Drugs* **2023**, *21*, 613. [CrossRef] [PubMed]
12. Islam, M.M.; Shahruzzaman, M.; Biswas, S.; Nurus Sakib, M.; Rashid, T.U. Chitosan based bioactive materials in tissue engineering applications-A review. *Bioact. Mater.* **2020**, *5*, 164–183. [CrossRef] [PubMed]
13. Rehman, K.U.; Hollah, C.; Wiesotzki, K.; Heinz, V.; Aganovic, K.; Rehman, R.U.; Petrusan, J.-I.; Zheng, L.; Zhang, J.; Sohail, S.; et al. Insect-Derived Chitin and Chitosan: A Still Unexploited Resource for the Edible Insect Sector. *Sustainability* **2023**, *15*, 4864. [CrossRef]

14. Mohan, K.; Ganesan, A.R.; Muralisankar, T.; Jayakumar, R.; Sathishkumar, P.; Uthayakumar, V.; Chandirasekar, R.; Revathi, N. Recent insights into the extraction, characterization, and bioactivities of chitin and chitosan from insects. *Trends Food Sci. Technol.* **2020**, *105*, 17–42. [CrossRef] [PubMed]
15. Esfahani, A.G.; Sartori, M.; Bregoli, C.; Fiocchi, J.; Biffi, C.A.; Tuissi, A.; Giavaresi, G.; Presentato, A.; Alduina, R.; De Luca, A.; et al. Bactericidal Activity of Silver-Doped Chitosan Coatings via Electrophoretic Deposition on Ti6Al4V Additively Manufactured Substrates. *Polymers* **2023**, *15*, 4130. [CrossRef] [PubMed]
16. Ramezani, M.; Ripin, Z.M. An Overview of Enhancing the Performance of Medical Implants with Nanocomposites. *J. Compos. Sci.* **2023**, *7*, 199. [CrossRef]
17. Barabadi, H.; Jounaki, K.; Pishgahzadeh, E.; Morad, H.; Sadeghian-Abadi, S.; Vahidi, H.; Hussain, C.M. Antiviral potential of green-synthesized silver nanoparticles. Handb Microb Nanotechnol. *Int. J. Nanomed.* **2022**, *14*, 285–310.
18. Nie, P.; Zhao, Y.; Xu, H. Synthesis, applications, toxicity and toxicity mechanisms of silver nanoparticles: A review. *Ecotoxicol. Environ. Saf.* **2023**, *253*, 114636–114648. [CrossRef] [PubMed]
19. Srikar, S.K.; Giri, D.D.; Pal, D.B.; Mishra, P.K.; Upadhyay, S.N. Green Synthesis of Silver Nanoparticles: A Review. Green and Sustainable Chemistry. *Green Sustain. Chem.* **2016**, *6*, 34–56. [CrossRef]
20. Jiang, Z.; Li, L.; Huang, H.; He, W.; Ming, W. Progress in Laser Ablation and Biological Synthesis Processes: "Top-Down" and "Bottom-Up" Approaches for the Green Synthesis of Au/Ag Nanoparticles. *Int. J. Mol. Sci.* **2022**, *23*, 14658. [CrossRef]
21. Zeng, H.; Du, X.; Singh, S.C.; Kulinich, S.A.; Yang, S.; He, J.; Cai, W. Nanomaterials via laser ablation/irradiation in liquid: A review. *Adv. Funct. Mater.* **2012**, *22*, 1333–1353. [CrossRef]
22. Triunfo, M.; Tafi, E.; Guarnieri, A.; Salvia, R.; Scieuzo, C.; Hahn, T.; Zibek, S.; Gagliardini, A.; Panariello, L.; Coltelli, M.B.; et al. Characterization of chitin and chitosan derived from *Hermetia illucens*, a further step in a circular economy process. *Sci. Rep.* **2022**, *12*, 6613. [CrossRef] [PubMed]
23. Chen, Q.; Cabanas-Polo, S.; Goudouri, O.M.; Boccaccini, A.R. Electrophoretic co-deposition of polyvinyl alcohol (PVA) reinforced alginate-Bioglass® composite coating on stainless steel: Mechanical properties and in-vitro bioactivity assessment. *Mater. Sci. Eng. C* **2014**, *40*, 55–64. [CrossRef] [PubMed]
24. Dvorakova, J.; Wiesnerova, L.; Chocholata, P.; Kulda, V.; Landsmann, L.; Cedikova, M.; Kripnerova, M.; Eberlova, L.; Babuska, V. Human cells with osteogenic potential in bone tissue research. *Biomed. Eng. Online* **2023**, *22*, 33. [CrossRef] [PubMed]
25. Fernández-Arias, M.; Boutinguiza, M.; del Val, J.; Medina, E.; Rodríguez, D.; Riveiro, A.; Comesaña, R.; Lusquiños, F.; Gil, F.; Pou, J. RE-irradiation of silver nanoparticles obtained by laser ablation in water and assessment of their antibacterial effect. *Appl. Surf. Sci.* **2019**, *473*, 548–554. [CrossRef]
26. Kumirska, J.; Czerwicka, M.; Kaczyński, Z.; Bychowska, A.; Brzozowski, K.; Thöming, J.; Stepnowski, P. Application of spectroscopic methods for structural analysis of chitin and chitosan. *Mar. Drugs* **2010**, *8*, 1567–1636. [CrossRef] [PubMed]
27. Naito, P.K.; Ogawa, Y.; Kimura, S.; Iwata, T.; Wada, M. Crystal transition from hydrated chitosan and chitosan/monocarboxylic acid complex to anhydrous chitosan investigated by X-ray diffraction. *J. Polym. Sci. Part. B Polym. Phys.* **2015**, *53*, 1065–1069. [CrossRef]
28. Arima, Y.; Iwata, H. Effect of wettability and surface functional groups on protein adsorption and cell adhesion using well-defined mixed self-assembled monolayers. *Biomaterials* **2007**, *28*, 3074–3082. [CrossRef]
29. Heise, S.; Forster, C.; Heer, S.; Qi, H.; Zhou, J.; Virtanen, S.; Lu, T.; Boccaccini, A.R. Electrophoretic deposition of gelatine nanoparticle/chitosan coatings. *Electrochim. Acta* **2019**, *307*, 318–325. [CrossRef]
30. Pawłowski, Ł.; Bartmański, M.; Strugała, G.; Mielewczyk-Gryń, A.; Jazdzewska, M.; Zieliński, A. Electrophoretic deposition and characterization of chitosan/eudragit E 100 coatings on titanium substrate. *Coatings* **2020**, *10*, 607. [CrossRef]
31. Cometa, S.; Bonifacio, M.A.; Baruzzi, F.; de Candia, S.; Giangregorio, M.M.; Giannossa, L.C.; Dicarlo, M.; Mattioli-Belmonte, M.; De Giglio, E. Silver-loaded chitosan coating as an integrated approach to face titanium implant-associated infections: Analytical characterization and biological activity. *Anal. Bioanal. Chem.* **2017**, *409*, 7211–7221. [CrossRef]
32. Guarnieri, A.; Triunfo, M.; Scieuzo, C.; Ianniciello, D.; Tafi, E.; Hahn, T.; Zibek, S.; Salvia, R.; Salvia, R.; Falabella, P. Antimicrobial properties of chitosan from different developmental stages of the bioconverter insect *Hermetia illucens*. *Sci. Rep.* **2022**, *12*, 8084. [CrossRef] [PubMed]
33. Xie, H.; Wang, P.; Wu, J. Effect of exposure of osteoblast-like cells to low-dose silver nanoparticles: Uptake, retention and osteogenic activity. *Artif Cells Nanomed. Biotechnol.* **2019**, *47*, 260–267. [CrossRef]
34. Fazio, E.; Gökce, B.; De Giacomo, A.; Meneghetti, M.; Compagnini, G.; Tommasini, M.; Waag, F.; Lucotti, A.; Zanchi, C.G.; Ossi, P.M.; et al. Nanoparticles Engineering by Pulsed Laser Ablation in Liquids: Concepts and Applications. *Nanomaterials* **2020**, *10*, 2317. [CrossRef] [PubMed]
35. Menazea, A.A.; Ahmed, M.K. Wound healing activity of Chitosan/Polyvinyl Alcohol embedded by gold nanoparticles prepared by nanosecond laser ablation. *J. Mol. Struct.* **2020**, *1217*, 128401. [CrossRef]
36. De Bonis, A.; Sansone, M.; D'Alessio, L.; Galasso, A.; Santagata, A.; Teghil, R. Dynamics of laser-induced bubble and nanoparticles generation during ultra-short laser ablation of Pd in liquid. *J. Phys. D* **2013**, *44*, 445301. [CrossRef]
37. Avcu, E.; Baştan, F.E.; Abdullah, H.Z.; Rehman, M.A.U.; Avcu, Y.Y.; Boccaccini, A.R. Electrophoretic deposition of chitosan-based composite coatings for biomedical applications: A review. *Prog. Mater. Sci.* **2019**, *103*, 69–108. [CrossRef]

38. Kumari, S.; Tiyyagura, H.R.; Pottathara, Y.B.; Sadasivuni, K.K.; Ponnamma, D.; Douglas, T.E.L.; Skirtach, A.G.; Mohan, M.K. Surface functionalization of chitosan as a coating material for orthopaedic applications: A comprehensive review. *Carbohydr. Polym.* **2021**, *255*, 117487–117503. [CrossRef]
39. Govindaraj, S.; Sundaram Muthuraman, M. Systematic Review on Sterilization Methods of Implants and Medical Devices. *Int. J. ChemTech Res.* **2015**, *8*, 897–911.
40. Grząbka-Zasadzińska, A.; Amietszajew, T.; Borysiak, S. Thermal and mechanical properties of chitosan nanocomposites with cellulose modified in ionic liquids. *J. Therm. Anal. Calorim.* **2017**, *130*, 143–154. [CrossRef]
41. Shirosaki, Y.; Tsuru, K.; Hayakawa, S.; Osaka, A.; Lopes, M.A.; Santos, J.D.; Fernandes, M.H. In vitro cytocompatibility of MG63 cells on chitosan-organosiloxane hybrid membranes. *Biomaterials* **2005**, *26*, 485–493. [CrossRef]
42. Khalili, A.A.; Ahmad, M.R. A Review of cell adhesion studies for biomedical and biological applications. *Int. J. Mol. Sci.* **2015**, *16*, 18149–18184. [CrossRef] [PubMed]
43. Zhang, Z.; Cheng, X.; Yao, Y.; Luo, J.; Tang, Q.; Wu, H.; Lin, S.; Han, C.; Wei, Q.; Chen, L. Electrophoretic deposition of chitosan/gelatin coatings with controlled porous surface topography to enhance initial osteoblast adhesive responses. *J. Mater. Chem. B.* **2016**, *4*, 7584–7595. [CrossRef]
44. Souza, P.R.; de Oliveira, A.C.; Vilsinski, B.H.; Kipper, M.J.; Martins, A.F. Polysaccharide-based materials created by physical processes: From preparation to biomedical applications. *Pharmaceutics* **2021**, *13*, 621. [CrossRef] [PubMed]
45. Paul, W.; Sharma, C.P. Chitosan and Alginate Wound Dressings: A Short Review. *Trends Biometerials Artif. Organs.* **2004**, *18*, 18–23.
46. Amaral, I.F.; Cordeiro, A.L.; Sampaio, P.; Barbosa, M.A. Attachment, spreading and short-term proliferation of human osteoblastic cells cultured on chitosan films with different degrees of acetylation. *J. Biomater. Sci. Polym.* **2007**, *18*, 469–485. [CrossRef]
47. Lallukka, M.; Houaoui, A.; Miola, M.; Miettinen, S.; Massera, J.; Verné, E. In vitro cytocompatibility of antibacterial silver and copper-doped bioactive glasses. *Ceram. Int.* **2023**, *49*, 36044–36055. [CrossRef]